

Design and Testing of a Space Mechanism for Tether Deployment

Carlo Menon*

ESA, 2201 AZ Noordwijk, The Netherlands

Michiel Kruijff†

Delta-Utec, 2312 TT Leiden, The Netherlands

and

Antonios Vavouliotis‡

University of Patras, 265 00 Patras, Greece

DOI: 10.2514/1.23454

A mechanism for control of space tether deployment is presented and discussed in this paper. This friction device, called the “barberpole,” was derived from the textile industry. The mechanism was analyzed, developed, and tested for the second Young Engineers’ Satellite mission (YES2), which is intended to feature the first European tether deployment. YES2 further aims to use the tether to accurately deorbit a small innovative reentry capsule. The barberpole is used for precisely guiding the dynamics of a capsule by controlling the deployment velocity of a tether that connects the capsule to an orbiting platform, in this case the Foton satellite. Design steps, derivation of a mathematical model, thermal analysis, and experimental results of the device are presented in this paper. The exponential dependency of applied friction force vs number of tether wraps around the pole is theoretically and experimentally proved. Friction performance and predictability are discussed based on experiments performed both on ground using a custom-built test rig and during parabolic flight campaigns. The work highlights the suitability of the barberpole design for space tether applications.

Nomenclature

a	= acceleration, m/s ²
C_p	= specific heat capacity, J/g · °C
d	= tether diameter, m
FR	= centrifugal force, N
F _z	= vertical force, N
F _φ	= tangential force, N
f	= friction coefficient
J _p	= planetary radiation intensity, W/m ²
J _s	= solar radiation intensity, W/m ²
l	= pole length, m
m	= mass, kg
N	= normal force per unit length, N/m
n	= number of pole turns
r	= pole radius, m
s	= length tether on pole, m
T	= tether tension, N
Tensionin	= T tilted over $-\theta$ with the direction of ds , N
Tensionout	= $T + dT$ tilted first over $d\phi$ and then over $\theta + d\theta$, N
v	= tether velocity, m/s
x'	= dx/dt
θ	= helix angle variable, rad
ρ	= linear tether density, kg/m
ϕ	= turn angle, rad

\int_0, π = integral from 0 to π

Introduction

THE Second Young Engineers’ Satellite (YES2) is to perform Europe’s first tether deployment to demonstrate a payload transport system from a space station or orbiting platform to Earth by means of a swinging tether and an inflatable capsule [1–3]. Tether technology provides an alternative means for a frequent sample return service from space that could be performed with low mass, low volume, and little storage risk, by doing away with the need for attitude control and deorbit thruster systems [1,4]. The tethered reentry principle is based on momentum exchange: a small capsule is inserted into its reentry trajectory while the orbiting platform gets a small up-boost. YES2 could open up the way to this and other near-term tether applications that use momentum transfer. To be competitive with conventional solutions, an accurate landing spot should be achieved. It is believed that this is feasible through the use of very simple and lightweight tether deployer hardware, in combination with a robust tether deployment control strategy. The YES2 mission phases that should lead to a precise deorbit are summarized in Fig. 1: A) the tether is deployed and then braked, B) the tether swings back underneath the satellite platform, C) the tether is cut and the capsule is thus released, D) the capsule reenters towards the Earth.

The mechanism described in this paper is a friction brake developed for the YES2 with the purpose of reliably controlling tension in a 30-km tether during its deployment, and thereby accurately controlling the trajectory of a subsatellite suspended from the tether. The brake design should avoid tether jam that could lead to bounceback of the subsatellite and potential collisions. It should also not damage the tether, because an accidental severing would lead to a considerable debris issue. The brake is thus a critical part of the tether deployer design. The selected principle is called a “barberpole,” a simple pole around which the tether can be wrapped for controllable friction levels without the need for moving guides. The barberpole’s friction behavior depends exponentially on the number of tether wraps around the pole, as mentioned in [5] and derived in [6]. This allows for a large range of tension levels to be applied, which is

Presented at the 56th International Astronautical Congress 2005, Fukuoka, Japan, 17–21 October 2005; received 24 February 2006; revision received 30 November 2006; accepted for publication 19 January 2007. Copyright © 2007 by Carlo Menon, Michiel Kruijff, and Antonios Vavouliotis. Published by the American Institute of Aeronautics and Astronautics, Inc., with permission. Copies of this paper may be made for personal or internal use, on condition that the copier pay the \$10.00 per-copy fee to the Copyright Clearance Center, Inc., 222 Rosewood Drive, Danvers, MA 01923; include the code 0022-4650/07 \$10.00 in correspondence with the CCC.

*Researcher, Advanced Concepts Team, ESA, and the Center of Studies and Activities for Space “CISAS—G.Colombo,” University of Padova, 35131 Padova, Italy. Member AIAA.

†Technical Director. Member AIAA.

‡Ph.D. Student, Department of Mechanical and Aeronautical Engineering.

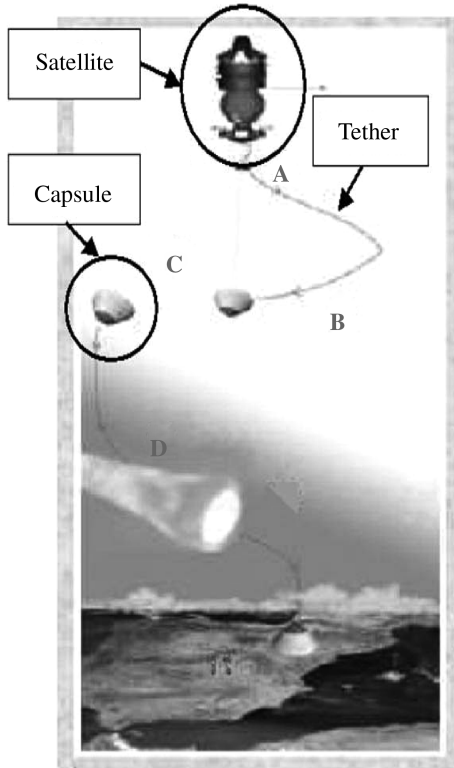


Fig. 1 Four mission phases. A: tether is deployed, B: tether swings back, C: tether is cut, and D: the capsule reenters.

required for proper control at very short (300 m) and very long (30 km) tether lengths under associated gravity-gradient forces. This paper seeks to determine the limits of applicability of such simple models both by analysis and test, and to increase the understanding of the brake's friction performance under the various circumstances that may be encountered in the space environment. The aim of this paper is furthermore to document the mechanical design tradeoffs for YES2's implementation of this concept.

The barberpole has been designed taking advantage of the experience and know-how of the textile industry [7]. Friction brakes have been used in the textile industry to introduce a constant tension level in yarns or fibers. There are no open or moving guides and the yarn is not compressed or damaged by the braking mechanism. First successes of tether brakes using this principle in space were the SEDS1 and SEDS2 (small expendable deployer system) missions [8–10]. In these missions, 20 km of tether were deployed. A third SEDS brake system was included on ESA's YES1, the first satellite to feature a failsafe multistrand tether. This record-breaking 35-km tether [11] was, however, not deployed, due to safety issues [12]. In Europe, the SEDS system was used as an example for the control system in the "Tether System Experiment" (TSE) project [13]. The TSE and SEDS brakes have a relatively small sleek pole compared to the design in this paper. The motor that drives the gear is fixed directly to the housing, such that a highly precise alignment is required to allow for proper operation. One of the reasons to use a stepper motor is that the motor can be driven in open loop; there is no encoder. Tests were performed for TSE, but the project was eventually canceled. In one high-speed/high-tension test, the tether melted. Then, after the YES1 and TSE projects, it was found that reliability, thermal performance, performance predictability, and robustness could not be properly demonstrated for the earlier designs and it was therefore obligatory to develop and qualify from scratch a new barberpole brake system for the European Space Agency. The innovative value of the new European system described in this paper lies in the increased understanding and optimization of the concept's performance as a result of design tradeoffs, analysis, and tests performed. The YES2 mission explicitly requires a strict tether deployment control and a high level of safety. A better mathematical

understanding was required to help understand under which conditions performance would be maintained. The mathematical model has led to a new dimensioning of the pole, with more uniform performance, as well as reduced entry guide distance to the pole for more efficient use of the increased dimension, and finally a curvature in the pole surface that is intended to help stabilize the tether motion on the pole. Surface treatment effects were studied to come to a clear manufacturing procedure. In addition, when the deploying tether is in contact with the barberpole and subjected to high friction in vacuum, the tether can easily melt, causing the failure of the mission. The new design is therefore for a significant part driven by increased thermal dissipation. An extra guide and reliaflex coupling were added to the brake system to decrease misalignment torques. Systematic analyses and tests of the braking mechanism were carried out.

In the first part of this paper, the main requirements for and characteristics of the barberpole are presented and a mathematical model is described. Possible solutions for barberpole configurations are shown and pros and cons of each configuration are discussed. A thermal analysis is then presented to verify that the tether will not melt during the deployment phase. A barberpole breadboard was developed and the experiments performed with it are discussed. The paper ends with a conclusion on the understanding of the performance and the suitability of the tested barberpole for YES2.

Problem Definition

The objective of the YES2 mission is to demonstrate a safe and precise capsule reentry using tether technology. To be an interesting cost-effective alternative to conventional solutions, the system should be compact and reliable. Therefore, we strive for subsystems that are simple, well-tested, and with few interfaces. Awareness of risks and contingencies is a key point for the success of the mission; failures and abort options must be identified and evaluated. In particular, the barberpole should be lightweight and easy to manufacture. Performance should be predictable and replicable, and variations in parameters should be able to be compensated for via feedback. It should be effective in a wide range of tension levels, so an exponential performance is preferred. For reliability and safety it should have few moving parts and few tether guides. The design should effectively conduct heat away from the friction surface. Performance should be understood and demonstrated in all foreseeable circumstances.

These requirements led to the selection of a barberpole concept. Figure 2 shows a tether wound four times around a pole. The tension of the tether increases approximately three times for each turn of the tether around the pole, as will be shown in the next section. At the entrance hole of the braking tether pole, the tension is about 10 mN. It is nonzero because the tether must first be unwound and accelerate from a storage spool inside a box (canister).

Therefore, four turns around the brake introduce a tether tension at the exit hole (see Fig. 2) of almost 1 N. The dynamic of the space mission requires a tether tension from 10 mN (no turns) to 3 N (about four turns). The difficult characterization of the tether dynamics during braking operations has required the development of a robust deployment control algorithm and the construction of a real-time tether deployment test rig, which was developed at the University of Applied Sciences Koblenz in Remagen (Germany).

In Fig. 2, the entrance and exit holes are fixed to the pole, thus preventing control of the tether deployment speed. It is therefore necessary to develop a more sophisticated mechanism that is able to change the number of turns around the pole to brake the tether in an effective way. The mechanism must also keep down the temperature of the tether to prevent its breakage. The tether foreseen for YES2 mission is a polyethylene wire, Dyneema, selected for its low density, high strength and stiffness, and smooth flexible surface. The characteristics of this material are shown in Table 1. Stiffness is highly dependent on usage, tension history, and load and as a result can easily vary by a factor of 10 from one application to the next [13]. Because of the low tension levels and high material strength, the diameter of the tether is determined by the meteorite cutting risk, and was fixed at 0.5 mm.

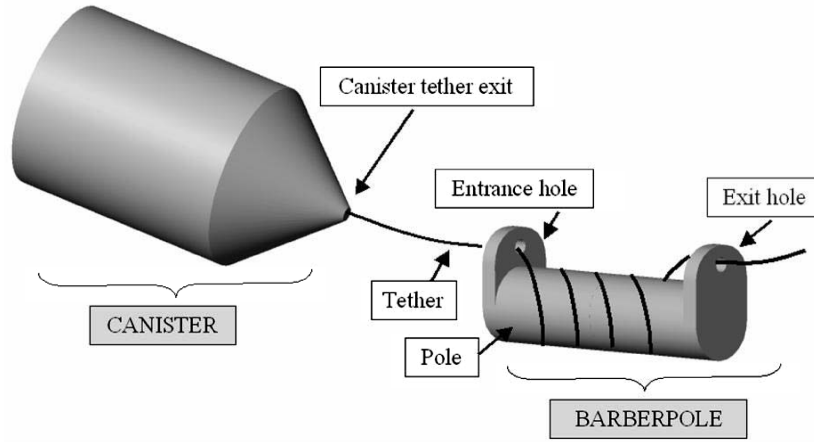


Fig. 2 Canister and braking tether pole.

Mathematical Model

As mentioned, the exponential dependency of applied friction force vs number of tether wraps, or “turns,” around the pole is beneficial for control. In the required large range of deployment tension, such a model would allow for a simple linear control algorithm. By using the mathematical model described in this chapter and performing experiments on different kind of barberpoles, the deviation from a pure exponential dependency between friction force and pole turns was assessed.

The mathematical model of the barberpole braking performance (see Appendix for details) was based on several important assumptions. In particular, the velocity v of the tether around the pole is assumed constant, the tether density ρ is constant, the tether entry and exit points are fixed and located on the extremities of the pole, the incoming and outgoing angles of the tether can change, the pole radius r is constant, and the tether has no bending stiffness.

The first conclusion, which is drawn from the mathematical model under the aforementioned assumptions, is that the tether should assume the shape of a helix (θ is constant). Hence, the helix angle θ can be calculated from the number of turns and geometry of the pole:

$$\tan \theta = 1/2\pi nR \tag{1}$$

The length of the piece of moving tether instantaneously in contact with the pole equals

$$s = 1/ \sin \theta \tag{2}$$

Another important conclusion is that the tether should stay in contact with the pole if the normal force remains positive. This statement is true if and only if the incoming tension T meets the condition $T > \rho v^2$. This condition is intuitively understood as the inertia of the tether has to be overcome.

The term ρv^2 is known as the “rocket term” [14]. This term equals the tension that will occur in a tether due to the energy shock (Carnot) that it experiences when making the transition from being stored on a fixed spool to deploying at constant velocity. Because YES2 will have such a spool, the tether tension will include a rocket term. The tension at the entrance of the barberpole will be an amplified version of this term, due to bending around guidance surfaces and friction forces encountered along the way.

Therefore, the condition $T > \rho v^2$ is always met and implies that a nonstiff tether deployed from a spool at constant velocity will be in contact with the barberpole brake regardless of density or deployment speed. This conclusion does not hold for stiff tethers (required bending moments will set a tougher condition to meet), nor necessarily for decelerating deployment (inertia effects of tether at the low friction end). Strongly decelerating deployment in a typical deployment is initiated by the barberpole friction itself rather than by reduced gravity gradient (or sudden stop of a test-rig reeling mechanism), so probably deceleration will not give any problems for the tether/pole contact.

The third conclusion from the mathematical model is that the tension in the tether as it leaves the barberpole is nearly proportional to incoming tension and depends nearly exponentially on the turn angle ϕ and friction coefficient f , according to

$$T = (T_0 - \rho v^2)e^{\cos \theta \int f d\phi} + \rho v^2 \tag{3}$$

This equation has interesting implications for the system physics. Notice that this formula contains the rocket term, even though shock accelerations were not part of the model. It predicts, however, that the rocket term passes the brake unamplified. For constant friction coefficient f the formula simplifies to

$$T = (T_0 - \rho v^2)e^{2\pi f n \cos \theta} + \rho v^2 \tag{4}$$

Or, expressed in geometrical design parameters,

$$T = (T_0 - \rho v^2)e^{2\pi f n \sqrt{(1/\{1+[1/2\pi n/(r+0.5d)]^2\})}} + \rho v^2 \tag{5}$$

Figure 3 shows the predicted performance [Eq. (4)] relative to an idealized exponential barberpole ($T = T_0 e^{2\pi f n}$). Plots are for three different friction coefficients: $f = 0.1, 0.18,$ and 0.3 . The vertical axis is relative performance ($1 =$ idealized exponential), with steps of 5%. Horizontal (back-to-front): number of brake turns, with steps of 0.25 turn. The lower axis extreme of 1 corresponds to zero turns, the upper value of 21 corresponds to five turns. Horizontal (left-to-right) is pole ratio (radius/length), where s1 corresponds to a ratio of 0, and s11 to 0.25; steps of 2.5%. Behavior relative to a simple exponential also depends on the friction coefficient. A relatively thicker pole is better and a lower friction coefficient more closely approaches the ideal result (no relative losses due to helix angle). Losses are largest at ~one turn: ~40%. For higher friction coefficients, the effect is more pronounced. For poles with a diameter > 0.25 length (curves on back wall), performance is generally better than 80%, so a simple exponential fit will suffice. Thinner poles, however, have heavily degraded performance (left-side curves).

Table 1 Dyneema characteristics

Physical properties	Fiber	YES2 tether
Density	970 kg/m ³	915 kg/m ³
Tensile strength, ultimate	3500 MPa	500–1500 Mpa
Modulus of elasticity	110 Gpa	~25 GPa
Onset of performance degradation	~70°C	~70°C
Maximum usage	~120°C	~120°C
Melting temperature	150°C	150°C

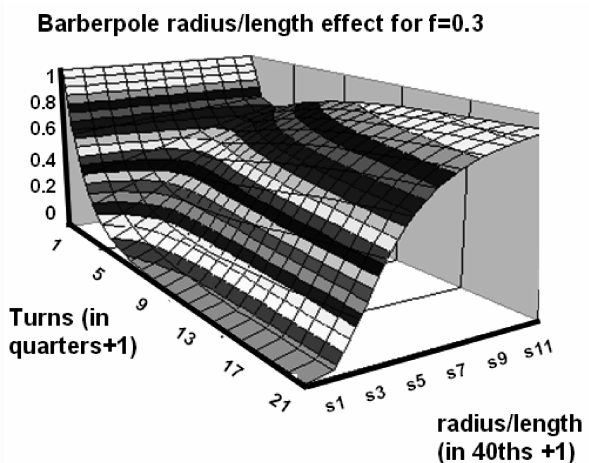
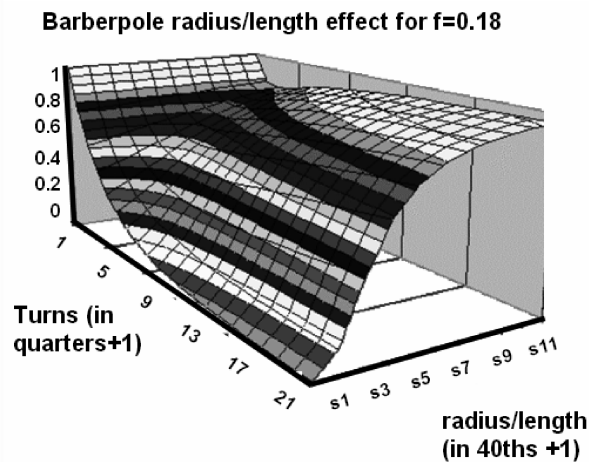
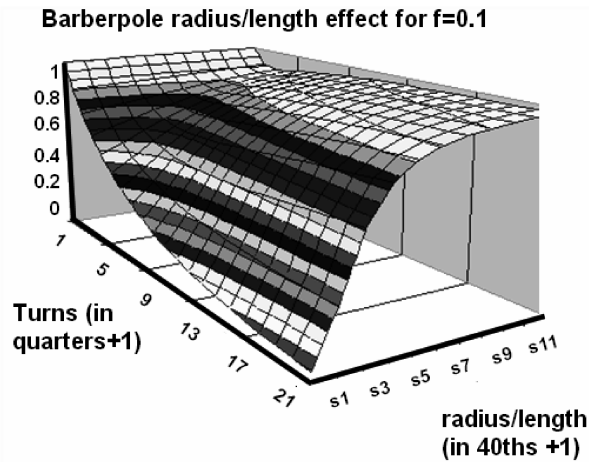


Fig. 3 Predicted friction performance [Eq. (4)].

Barberpole Design

With the required exponential behavior established for the barberpole concept, several configurations have been designed to obtain a high-performance barberpole. In this section, the most promising solutions are presented. Figure 4 shows the first configuration of barberpole, which is made up of three main components: one motor, one pole, and one external cover. This configuration can be very compact and reliable because only a few components are used. The motor turns the pole around its axis and winds the wire. To have a position of the mechanism in which the tether is allowed to move freely through the barberpole without actually touching it (zero friction), the entrance and exit holes are aligned. This constraint implies a complicated path for the winding tether (see Fig. 4) and complicates the dynamic model of the system

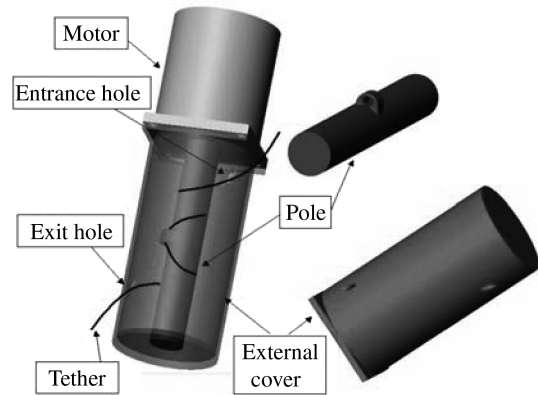


Fig. 4 First barberpole configuration.

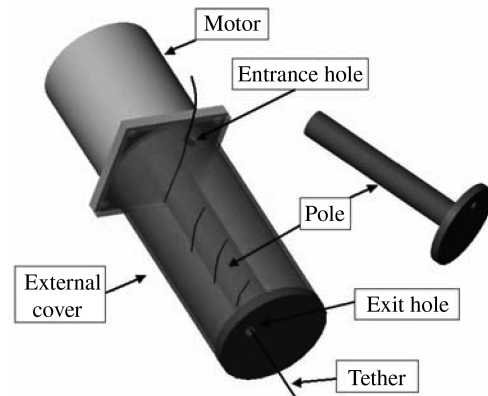


Fig. 5 Second barberpole configuration.

and the speed control of the tether. A torque is applied continuously by the tether directly on the motor, increasing system requirements. A second configuration is shown in Fig. 5. In this case, the exit hole is fixed to the end of the rotating pole and the tether winding path is more regular.

There are two inherent drawbacks for these two barberpole configurations. The first one is related to the mechanical rigidity. For both configurations, the pole is turned by the motor around its axis. Therefore, the pole behaves as a cantilever. A bearing system must therefore be employed to increase the mechanism stiffness necessary to withstand both the launch phase (random, quasi-static, and sinusoidal excitations) and the operational phase of the mission. The second drawback concerns the barberpole thermal behavior. In space, conduction and irradiation are the only two ways of transferring heat energy. In the aforementioned configurations, the pole must rotate to allow control of the tether speed. The use of bearings or other sliding systems is therefore needed. The total conduction of the barberpole is thus compromised and the possibility of melting the tether increased.

Other configurations were examined. Figures 6 and 7 show two barberpole geometries characterized by nonrotating poles. The tension and therefore the torque at entry is much smaller than at exit, so the entrance could easily be moved directly. The exit must preferably open into (free) space. In Fig. 6, the position of the tether entrance hole is controlled by a motor through a shaft. In Fig. 7, the motor directly guides a beam and the position of the tether entrance hole. By having a fixed pole, the thermal performance of these braking mechanisms is improved. When the barberpole is joined to a massive thermal sink, as in the YES2 mission, the heat produced by the friction between tether and pole can easily be dissipated. However, despite the notable advantages of these two configurations, their use was prevented by the YES2 mission constraints.

The first constraint was related to the small space available for the braking mechanism limiting its dimensions. The second constraint is the barberpole diameter. In fact, it must be noted that the entrance hole has a circular trajectory around the axis of the pole. A smaller

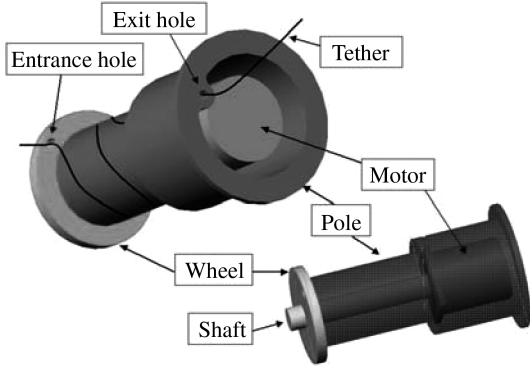


Fig. 6 Third barberpole configuration.

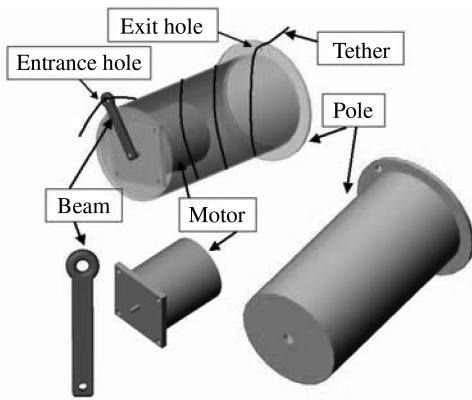


Fig. 7 Fourth barberpole configuration.

pole diameter is therefore preferred because it assures small position changes of the entrance hole with respect to the canister tether exit.

The final barberpole design for the breadboard model is shown in Fig. 8. This design, which is based on YES1’s SEDS deployer mechanism concept, is made up of a pole that is fixed to an external casing. The entrance hole is set on a tooth wheel, which is controlled by a motor that rotates a shaft and a worm gear.

The main differences with respect to the SEDS system are gear ratio (reducing required motor torque), motor fixture (increasing friction but allowing for misalignments), pole base design (large base for increased thermal conductivity and heat capacity), and pole dimensions and shape (based on model results and test recommendations). A second worm to reduce the tooth wheel’s freedom during launch was considered, but rejected as overdesign.

The main advantages of this configuration over the other concepts are manifold. In particular, the pole, ground plate, and guide are a single integrated piece. In addition, the barberpole is fixed to a frame (heat sink), which benefits thermal dissipation. This configuration has also a space-saving geometry. For this configuration a transmission mating mechanism is used for torque reduction, which

allows using a low power motor. The nonreversible worm/tooth-wheel transmission mating mechanism keeps the free rotations of the mechanism steady during the launch phase while no current is provided to the payload. Misalignments are compensated by using a flexible motor-axis connection

The technical characteristics of this final barberpole are as follows: Vespel, a low-friction polyimide, is used for the entrance guide. The exit guide is milled directly into the aluminum frame, for optimal heat transfer. Sliding bushes are employed at the rotating interfaces to reduce friction and present low failure probability. A stepper motor is preferred for its deterministic nature, allowing for open-loop software control. A space-qualified motor (Phytron VSS 32.200.1.2) is planned.

The worm/tooth-wheel mating, which is used to amplify the motor torque, has a reduction ratio equal to 120. An 8 kHz half-step mode allows winding of the tether around the pole once every 6 s, which is in accordance with mission requirements. Half-step mode leads to double frequency and extra power and torque loss, and is mainly selected to reduce vibration resonance losses within the motor.

Figure 8 also shows the tether-cutter mechanism. This barberpole submechanism is aimed at cutting the tether at the end of the deployment phase. It is made up of a holder and two redundant pyrocutters (Cypres AirTec).

Thermal Analysis

Introduction

The presented design was heavily influenced by thermal considerations, because melting of the Dyneema by friction heating was considered a serious risk. To evaluate the thermal behavior of the designed barberpole during the YES2 mission, a thermal analysis was performed using ThermXL provided by ALSTOM Co. For general applicability of this work, the barberpole assembly is assumed to be independent, not taking into consideration any mechanical or thermal interfaces with other YES2 subsystems. This assumption is conservative for the specific scenario of the YES2 mission as the hot case is of concern and the conductive interfaces with other subsystems will lead to additional cooling. The analysis performed takes into account the thermal environment of the low Earth orbit of FOTON [15] and also the tether deployment profile of the mission [16].

Modeling

A CAD design is used for the thermal analyses. The barberpole assembly is represented as a six-sided box with the stepper motor fixed on one side of the box. Inside the box there is the pole (cylinder and flange).

The entire assembly is modeled with 13 nodes (see Fig. 9 and Table 2). The parts that are modeled are the housing, the pole, and the motor. Every node is assumed to be in perfect contact with the adjoining nodes as if they were all from one part. Every external side of the box is an isothermal area, so every side of the box is a discrete node.

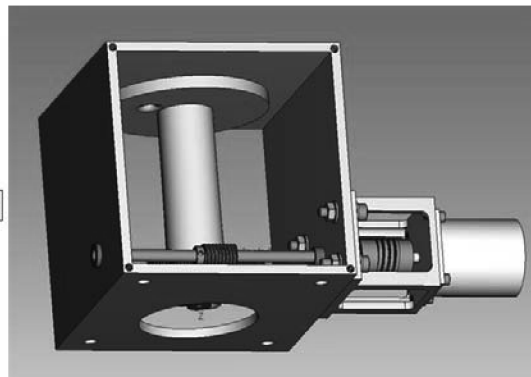
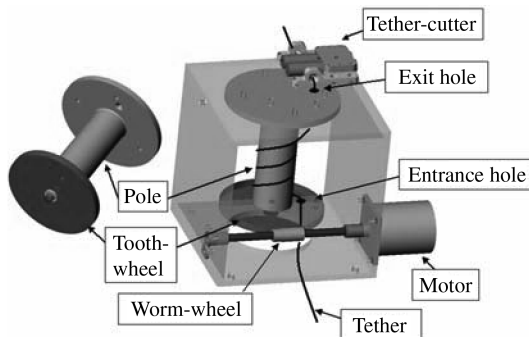


Fig. 8 Latest barberpole configurations. The first picture is the testing breadboard, which allows for easy testing of a variety of parameters. The second represents the flight design.

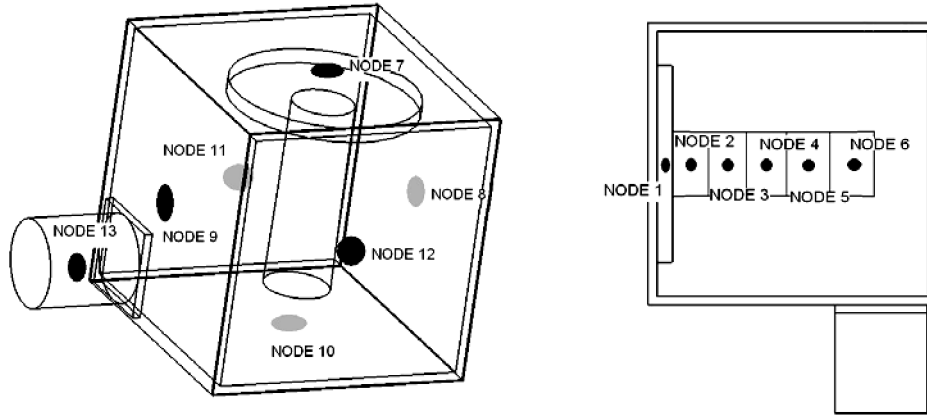


Fig. 9 Barberpole configuration and nodal breakdown.

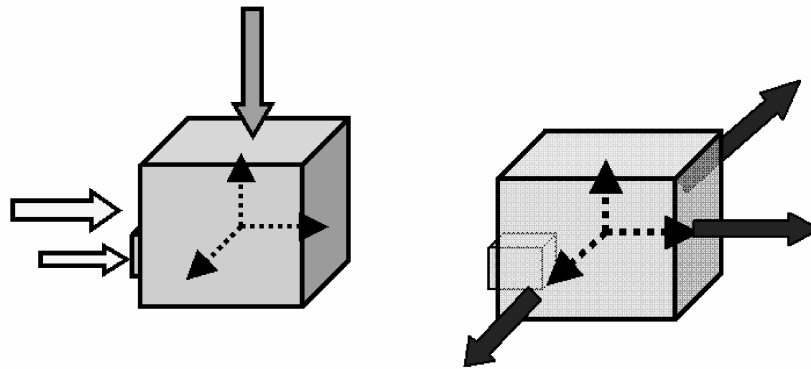


Fig. 10 Heat input/output.

Space Environment

We assume the worst scenario in which one side of the box absorbs radiation directly from the sun and a second (the top of the box) receives albedo and infrared from the Earth (see Fig. 10 and Table 3). Values concerning radiation heat input are calculated assuming that the satellite passes from full sun exposure to full eclipse (or spacecraft shadow) every 45 min (2700 s). In the worst-case scenario that is considered, the heat output is primarily considered to be coming from three sides of the assembly that are radiating to deep space. The conservative analysis performed does not consider the heat transfer between Foton/YES2 and the barberpole assembly.

The panel that receives the sunlight, the one with the stepper motor attached, is assumed to dissipate 5 W continuously. The heat input (dissipated power) given by the friction of the tether on the pole's surface is calculated by multiplying the tether's tension force by the tether's velocity. This product reaches a peak power of tens of Watts during the final minutes of deceleration. It is conservatively assumed that half of this heat input passes to the pole and the other half is equally distributed along the deployed length of the tether. This assumption is conservative because the tether is cooler than the pole, as it does not accumulate heat in passing. The dissipated power is distributed over the nodes of the pole according to Eq. (3), which will lead to input mostly into the tether exit in the pole base (node 1), which is bolted to the box (node 7). Values of the parameters are selected in a way to define a worst-case heating scenario so that they can give an indication of the robustness of the design.

The analysis performed is a transient one [17]. The analysis calculates the temperatures of the YES2 satellite for 20,800 s (covering startup and full deployment). The initial temperature is 0°C. The cyclic trends in the results are due to the eclipse that occurs every 90 min.

Thermal Analysis Results

The temperature changes are governed by the extremes of the orbital environmental circumstances. It can be seen (Fig. 11) that the

peak value occurs when the maximum tension on the pole is applied during the deceleration phase (Fig. 1) of the capsule (deceleration from 12 m/s to zero in few minutes). A rise of about 50 deg is caused by the braking action (as seen from increase in peak level). The housing also gets quite hot. The temperatures are within the acceptable range, even if the initial temperature will be lower in the real scenario. No conduction to the YES2 is assumed. The thermal performance of the pole itself (minimizing the influence of friction heat) can be further improved by applying thermal paste and bolting it tightly to the barberpole housing.

Breadboard for Experimental Tests

With the design completed and initial confidence obtained by analysis, a barberpole breadboard was built for experimental tests including friction and contact behavior, performance in zero-g and

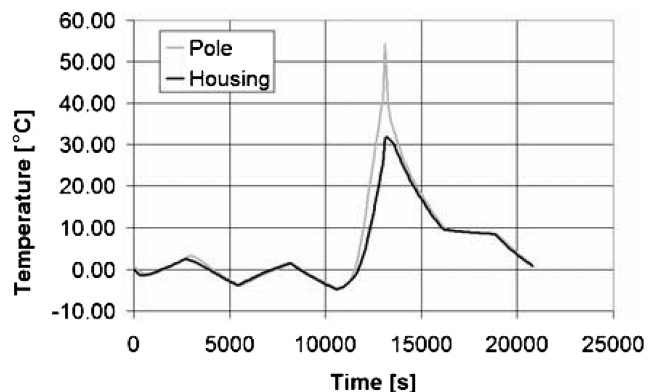


Fig. 11 Barberpole temperature estimation. Temperature within the pole itself varies less than 5°C.

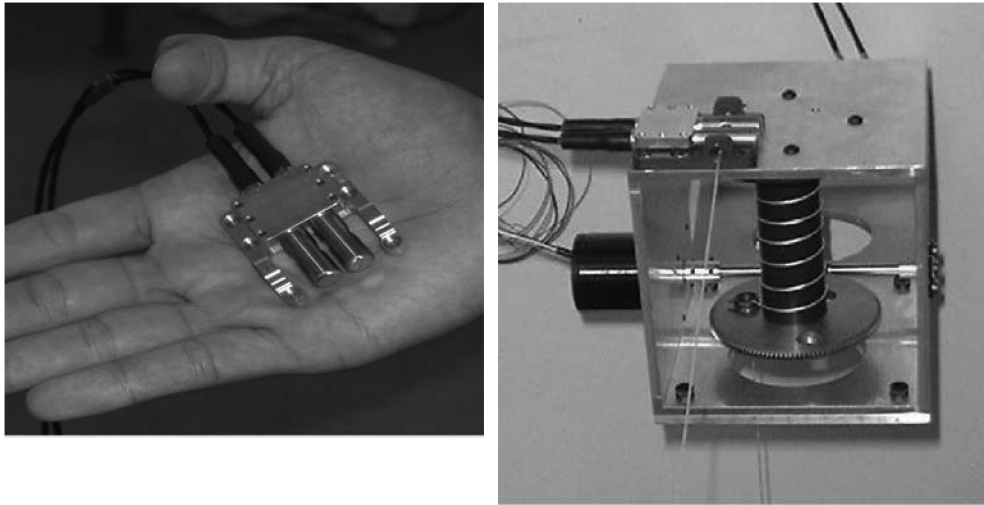


Fig. 12 Left: tether cutter. Right: barberpole (including pole “curved 1”).

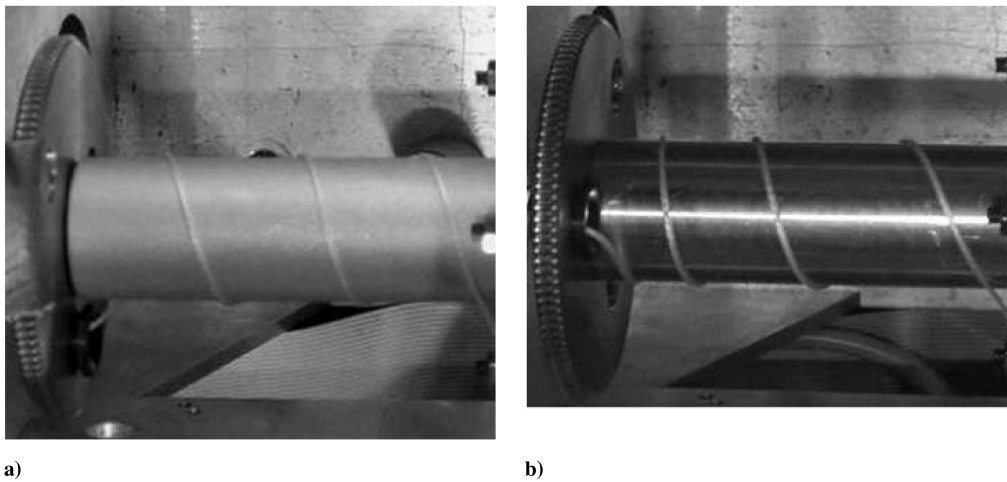


Fig. 13 Path of the tether around the sandblasted and smooth-surface wide diameter poles.

vacuum, and finally performance in a closed-loop control. Figure 12 shows the tether-cutter subsystem and the overall barberpole system. In Fig. 12, the tether goes through the entrance hole of the tooth wheel, turns six times around the pole and goes through the tether-cutter subsystem. The tether winds with a regular path around the barberpole as predicted in the mathematical analysis.

However, during preliminary tests, performed by means of a test-rig facility (discussed in the next section) that was especially developed for ground tests [7,18,19], the predicted helix shape was compromised, as the tether loops under some circumstances tended to collect near the entrance (compare Figs. 13a and 13b). In principle, this shape deviation is not an issue as the helix angle decreases for most turns and the braking effectiveness increases (the total contact length of tether with pole increases). However, in extreme cases, tether loops could overlap and, as a net result, friction output could be reduced significantly with respect to the exponential model. It would be even worse if some entanglement with tether or gear were to occur.

It seems that tether loops mostly overlap at a high number of turns (>2.5), on narrow poles with low surface roughness, with low incoming tension and thick tethers. Simple tests indicate that velocity and temperature seem not to be involved in the cause of the undesired effect. A methodological sequence of tests revealed that the observed behavior is the result of a combination of four contributions that we define as 1) internal torque (result of the braiding), 2) twist, 3) wrapping direction around the pole (it determines the direction of the previous effect), 4) pole tendency (a certain natural tendency of the pole, which is not yet understood but seems unaffected by any of the aforementioned parameters). We were able to qualitatively but

consistently define the relation between the separate effects as follows:

$$\begin{aligned} \text{Net torque effect on helix} &= (\text{twist} + \text{internal torque}) \\ & * \text{wrap direction} + \text{pole tendency} \end{aligned} \quad (6)$$

To identify the best diameter or surface treatment to match the models, several poles with different shapes and roughness were built and tested. The characteristics of the poles are summarized in Table 4. Surface roughness was determined using a Mitutoyo Surftest SV-3000. The measurements vary from ranges of 5–20 μm to ranges of 0.5–2.5 μm . The sandblasted poles were found to wear down during deployment tests, so a hard or anodized coating is advised.

One pole was manufactured that does not have a cylindrical shape but is tapered with a curve: it has a 24.2 mm diameter at the entrance hole and a 23 mm diameter near the exit hole. The section of the pole follows an arc profile with a 4 m radius as sketched in Fig. 14. This geometry was chosen to avoid the described collection of tether at the entrance hole, without driving the loops to the exit hole. The resulting semicone angle at entrance is 1 deg, an angle that is based on rough preliminary tests that show that the axial force component induced by this angle is sufficient to drive the loops towards the narrower end of the pole. The exit side of the pole is cylindrical (0 deg). A polished aluminum surface led to a perceived too-low friction coefficient, so the curved pole was tested with two different surface treatments.

Table 2 Geometrical and material data used

Housing		Pole		Stepper motor	
Number of nodes	6	Number of nodes	6	Number of nodes	1
<i>Geometrical data, m</i>					
Length of each primary side	0.1	Length of the pole	0.07	Length	0.032
Width of each primary side	0.1	Thickness flange	0.005	Width	0.032
Thickness of each primary side	0.003	Diameter of the pole	0.024	Thickness	0.039
Length of each secondary side	0.1	Diameter of the flange	0.07	Diameter	0.032
Thickness of each secondary side	0.0005	—	—	—	—
<i>Material data (Aluminium used)</i>					
Thermal conductivity	209 W/mK	Thermal conductivity	209 W/mK	Thermal conductivity	209 W/mK
Thermal conductivity between plates	200 W/m ² K	Thermal conductivity between plates	200 W/m ² K	Thermal conductivity between plates	200 W/m ² K
Density	2700 kg/m ³	Density	2700 kg/m ³	Density	2700 kg/m ³
Cp heat capacity (J/g · °C)	0.9	Cp (J/g · °C)	0.9	Cp (J/g · °C)	0.9
Absorptance (internal surface)	0.9	<i>a</i>	0.15	<i>a</i>	0.9
Emissance (internal surface)	0.9	<i>e</i>	0.9	<i>e</i>	0.9
Absorptance (external surface)	0.15	—	—	—	—
Emissance (external surface)	0.9	—	—	—	—

Table 3 Selected values for solar (Js) and planetary (Jp) radiation intensity

	Value	Unit
Js	1371	W/m ²
Jp (240 km orbit)	220	W/m ²

Table 4 Pole characteristics. Coating index: 1 = polished aluminium, 2 = hard anodized, 3 = hard coated, 4 = sandblasted-hard anodized-polished, 5 = sandblasted. Friction coefficient: see Sec.

Pole	Friction	Roughness, μm	Diameter, mm	Coating
1	0.15	0.57	24	3
2	0.24	0.76	17	3
3	0.18	0.64	13	3
4	0.18	0.59	17	1
5	—	0.75	13	1
6	—	0.7	24	4
7	0.34	1.74	24	5
8	0.28	1.92	17	5
9	0.3	2.26	13	5
Curved 1	0.21	—	24	2
Curved 2	0.25	2.7	24	4

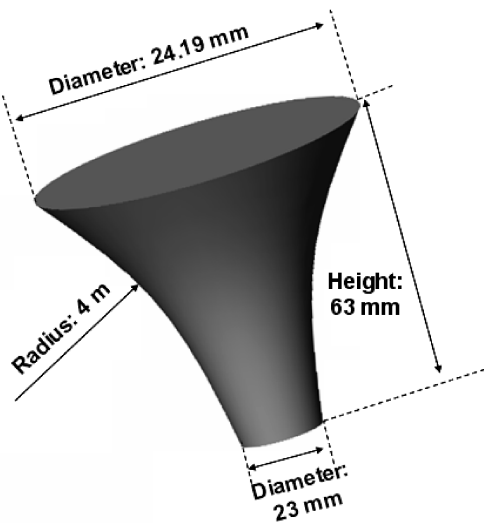


Fig. 14 Sketch of the section of the curved pole (exaggerated graphics of curvature).

Tests and Results

Friction Performance and Predictability

Ground tests were carried out using a custom-built facility, the test rig. Its main task was to pull the tether from the canister through the barberpole at the velocity that an ejected and separating capsule in the space environment would have. The main components of the test rig are shown in Fig. 15. Starting from the left of Fig. 15, the first two components are the satellite: tether canister (from which a tether deploys axially) and the barberpole. The third device is a tensiometer, which is able to measure the tension of the tether that exits the barberpole. This tension is a result of the barberpole's induced friction and is stored as data, but can also be sent to a real-time simulator that uses it inside a force balance in a simulated space environment. The fourth device is the galet, which is a motorized mechanism able to pull out the tether from the spool inside the canister, which is driven by the operator directly or by the real-time space simulator. The remaining components are buffers and sensors cooperating to recover the tether for reuse [12].

The ground experimental testbed thus allowed performance of extensive tests to verify both the control law and the barberpole performance. In this section the results concerning barberpole performance are shown and discussed.

During tests, the poles of Table 4 were mounted, in turn, on the barberpole. For each test, a fixed number of tether turns around the pole was used at a constant speed (1 m/s) and 1 km of tether, wound on a 70-mm-diam spool core, was employed. Each pole was tested in the range of 0–3.5 turns. The increment for successive experiments was 0.25 turns. Tether tension data were recorded with a frequency of 1 ms. Previous experience [12] has shown that the one-sigma noise around the tension averages at each number of turns amounts to about 30–40%.

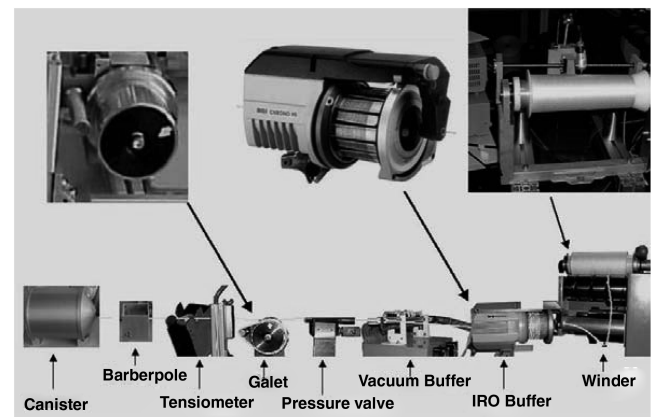


Fig. 15 Barberpole test rig.

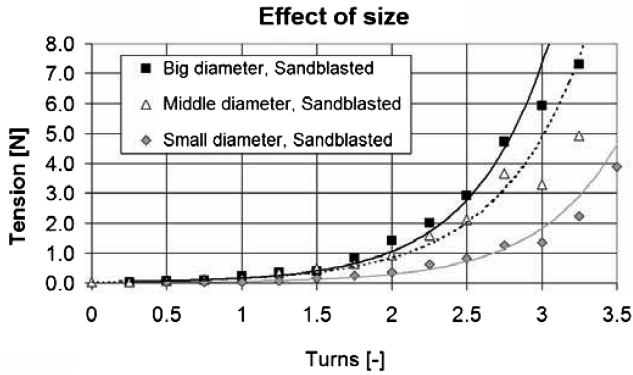


Fig. 16 Average tension of the tether for the three sandblasted poles, precision better than 0.1 N.

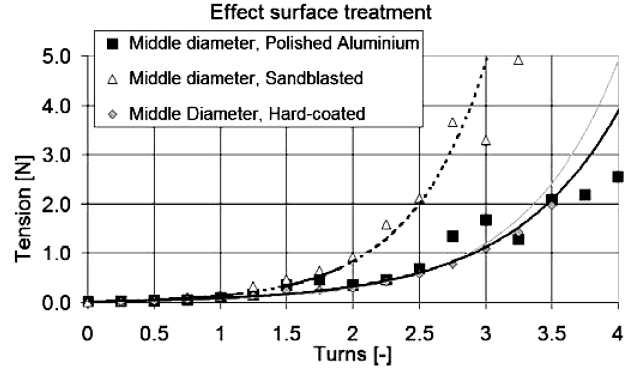


Fig. 18 Average tension of the tether for the middle diameter poles, precision better than 0.1 N.

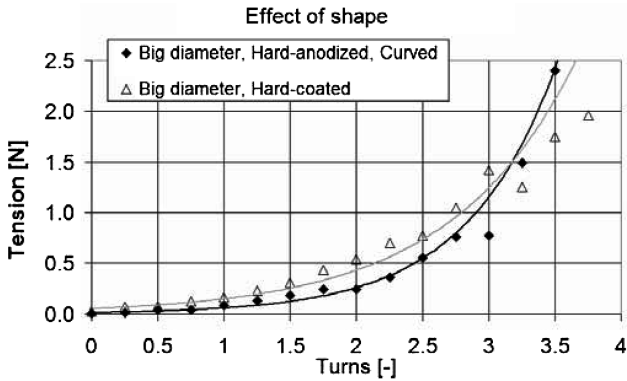


Fig. 17 Average tension of the tether for the coated big poles (cylindrical vs curved), precision better than 0.1 N.

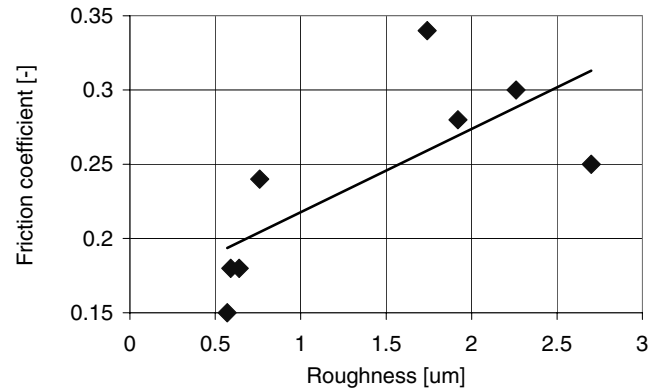


Fig. 19 Trend between roughness and friction coefficient.

Exponential fits are added to the data, from which the friction coefficient is estimated: the exponential coefficient of the tension curve divided by 2π [simplification of Eq. (3)]. Figure 16 shows results of the average tension of the tether for the three sandblasted poles. Especially for the sandblasted pole there seems to be a clear trend of increasing friction performance with pole diameter. According to the mathematical model, this effect would not so much be a true friction effect; rather it is improved tension amplification. Figure 17 shows experimental results concerning the two coated big poles, which differ mostly in shape (cylindrical vs curved). The curved pole seems to maintain its purely exponential behavior the longest, which is probably related to the fact that the cylindrical pole had an early onset of instability of the helix pattern (observed vibration of coils from about 2.5 turns). Figure 18 compares the exponentials for different surface treatments, and the sandblasted pole clearly stands out.

In general, the exponential shape is well followed until about $n = 3$ or 3.5. After that level, generally some relative losses in tension can be observed (except perhaps for the curved pole).

In Fig. 19, a trend between roughness and friction coefficient can be observed, which was found to be the main effect. Also the treatment can be found to have some influence (Fig. 20) although mostly for the sandblasted poles (Fig. 18). The various tests indicate a predictability of friction coefficient of about $\pm 20\%$, which should be taken into account in mission simulations.

Visual Observations

Figures 13a and 13b, respectively, show the path of the tether around the sandblasted and smooth-surface wide diameter poles. Whereas in Fig. 13a the tether winds around the pole with a quasi-perfect helicoid, in Fig. 13b the tether is gathered near the tooth wheel.

Visual observations consistently indicate that the homogeneity and regularity of tether winding around the pole can be maintained

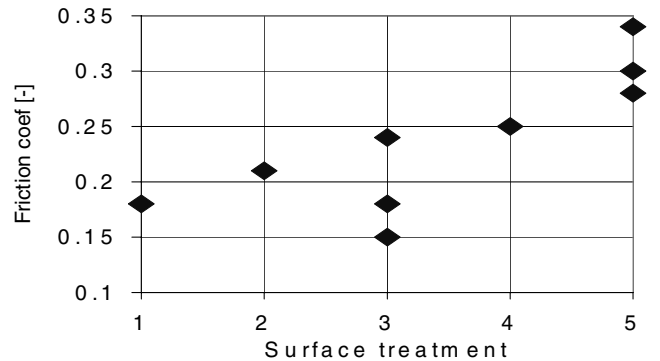


Fig. 20 Influence of the surface treatment on the friction coefficient of the poles. See Table 4 for surface treatment index.

for very large numbers of turns ($\gg 5$) by selecting the appropriate friction coefficient (>0.25), and/or by applying a mild curvature. However, having a too high friction coefficient or too high curvature can even lead to collection of loops on the exit side of the pole. The curvature leading to an entrance cone angle of 1 deg is (just) slightly too much.

Onset of instability was found to be directly associated with loss of performance. Its causes are as yet unclear, but its eventual solution is expected to extend the exponential performance to a larger number of turns. The sensitivity of the pole shape to tether twist indicates that seemingly small effects could be at the root of this remaining problem. Apart from the helix shape, tether irregularities, stiffness combined with localized twisting, and noise in incoming tension or in velocity are some directions for further study. As for now, in our further development of the deployment system we are trying to minimize all these potential causes. Then, especially with the hard-coated poles, it was observed that thinner poles seem to postpone the onset of instability, most likely because of the larger helix angle,

which makes them better than the bigger diameters. Somehow the coating may have some stabilizing influence compared to the smooth poles (Fig. 18).

Design Recommendations

It has been concluded that a surface roughness of 1–2.5 μm is required, because a polished surface has low friction coefficient, associated poor helix shape, and early onset of instability. A coating, preferably hard anodization, is required to avoid wear of the surface. A large pole length relative to tether diameter can be expected to reduce the risk of tether overlap. A larger pole diameter both experimentally and mathematically predicts better tension amplification performance. Thermally, a large pole heats up less. Some curvature can be introduced to avoid collection of the tether on the incoming side (also reducing risk of overlaps), delaying somewhat the onset of instability, but too much curvature could possibly cause collection on the exit side as well as instability.

The best performance is thus expected from the curved, hard anodized, large pole.

Barberpole's Performance in Extreme Cases

The barberpole-delivered tension was measured up to 25 N, even with very low incoming tension. Although the exponential model did not hold as well above five turns, the barberpole could apply sufficiently predictable tension up to 25 N, and most likely beyond (Fig. 21).

At very low velocities, the friction coefficient seemed to drop. The coefficient was found to be very low ($f_n = 0.12$ rather than the usual 0.25) at low speed (5 cm/s), but such results have to be interpreted carefully due to the possibility that tensiometers do not behave optimally at such low speeds. Furthermore, the tether deployment drive (gallet) does not deliver a constant/smooth velocity in this very low region. Such speeds effectively only occur at the end of the first stage deployment of YES2 (3 km), at which time a higher gain level is recommended for the software controller to account for it.

Performance in Vacuum

A drop-weight setup was built in a vacuum chamber (SSAU, Samara, Russia) as in Fig. 22. Vacuum level was about 5.10–2 mm Hg. The tether is draped over suspended metal rods to obtain a safe distance from the pole box, and allow for smooth sliding, thus creating the possibility to test the pole in horizontal configuration as displayed. Known weights are attached to each side, 2 and 20 g, the larger weight on the outgoing side. It is expected that the minimum tension amplification factor of 10 (20/2) required to keep the mass from dropping can be achieved by \sim two turns. The pole is driven (turned) by a controller setup outside the vacuum chamber. There is an observation window on either side. The drop height that can be witnessed is about 40 cm and typically takes \sim 10 s with the pole in critical setting (friction in balance with weight; minimal, smooth velocity).

The test was performed six times in air and four times in vacuum (Fig. 23). The results show virtually the same friction coefficient in the two cases ($0.26 \pm 20\%$ ambient vs $0.24 \pm 33\%$ vacuum). If either of the extremes of measured friction coefficients was to occur

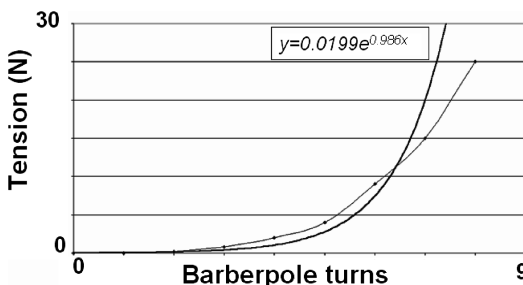


Fig. 21 Barberpole turns vs tension up to 25 N (actual data and exponential trend – $f_n = 0.16$).

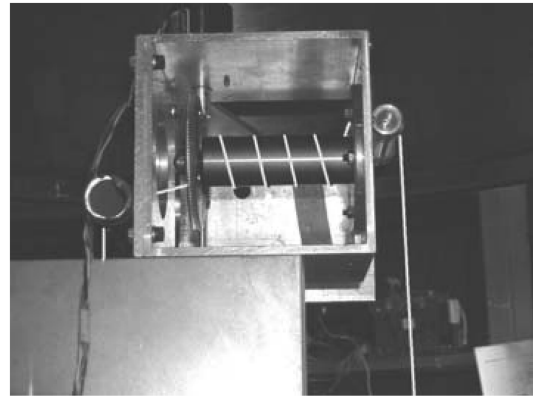


Fig. 22 Setup in vacuum chamber test. Incoming side on left, outgoing on right. Weights are suspended from the tether on either side (not visible). The tether path is highlighted for clarity.

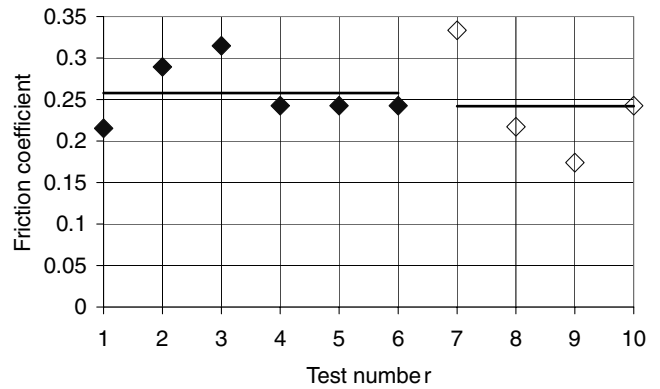


Fig. 23 Friction coefficient measured during six tests in air (solid dots) and four tests in vacuum (outlined dots), measurement error is better than 30% (approximately 1/4th of a turn).

as an average during a controlled deployment (in test or in space), a controller correction of 0.2 turns (ambient) or 0.4 turns (vacuum) would suffice to recover. These numbers seem valuable to take into account for mission safety/robustness simulations.

The vacuum measurements are noisier and the videos of the drop motion of the vacuum cases seemed much less uniform, suggesting that in vacuum at low speeds, stick-slip processes may be less reproducible.

Microgravity Environment

To verify correct deployment performance (unwinding of tether, entry of barber pole, and brake performance) in weightlessness, a parabolic flight experiment was performed by a YES2 student team as part of ESA's Fifth Student Parabolic Flight Campaign. The microgravity environment was obtained through two series of \sim 30 parabolic manoeuvres of a modified aircraft (Airbus A300 Zero-G). Each parabola was characterized by three main phases. Twenty seconds of 1.8 g ("pull up") is followed by the microgravity phase, also roughly 20 s, with an acceleration of $\pm 5 \times 10^{-2} g$ for the vertical axis (z axis) and $\pm 10^{-2} g$ along the x and y directions. After the microgravity phase, a 20-s vertical acceleration is reached once more, 1.8 g ("pull down").

The YES2 tether deployment test rig was specially prepared, and a vacuum cleaner replaced the tether recovery system to dispose of the deployed tether. The rig was run at 1 m/s for the duration of each parabola. The number of turns on the barberpole was increased in half steps only after every third test (\sim 150 m). Because of changes in the used spool's winding pattern over such distances, and related shifts in tension average, no reconstruction of an exponential behavior should be made, as done in the ground tests of the preceding section.

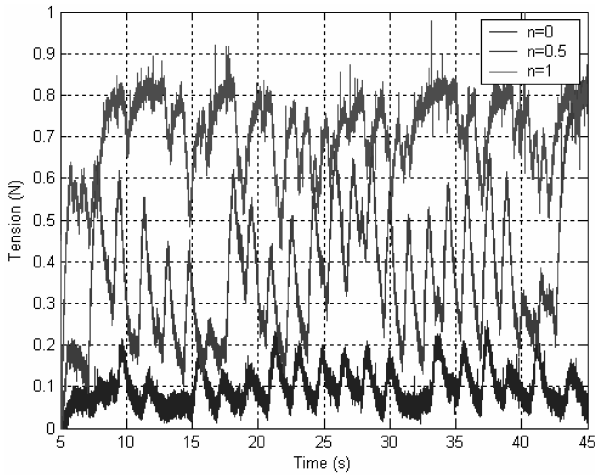


Fig. 24 Effectiveness of barberpole in microgravity. Criss-cross spool pattern.

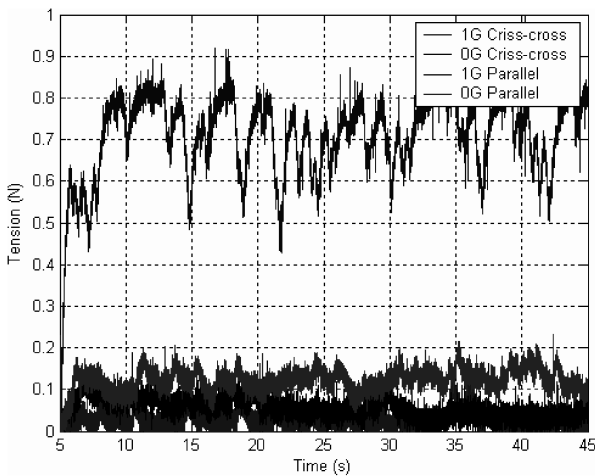


Fig. 25 Comparison of tension at different *g* loads and winding patterns.

Figure 24 shows the effectiveness of the barberpole in zero gravity when the tether is wound in a criss-cross pattern. Figure 25 shows a comparison of the tension using the two winding patterns for 0 and 1 *g*. The period of fluctuation in the deployment tension curves for tether wound in both criss-cross and parallel patterns matches the layer period of the spool windings used. Therefore it is likely that these cyclic tension patterns are due to the flange effect (touching of the spool core), as seen in ground tests [18].

Perhaps the most conclusive observation arises from the fact that only 21 s of each test involved microgravity. The first and last 10 s of each test were conducted at *g* levels ranging from 0 to 2 *g* (entry and exit from the parabola). There is no discernable difference in tension during these transitions. The position of the tether on the barberpole was also unchanged during the parabola. The results of the test show that the barberpole maintains its ability to function as a friction amplifier in 0 *g* and that the average tension did not change during each test, despite the changing *g* level.

A second parabolic flight experiment (43rd ESA Parabolic Flight Campaign) demonstrated the ability of the pole to deal with braking and restarting of deployment without entangling the accumulated wraps of tether on the pole.

Full Functional Test

A large number of full system tests were performed, in which the barberpole was coupled to the satellite breadboard and employed in a feedback control loop. The deployment test rig was run fully independently of the satellite breadboard (no information is shared

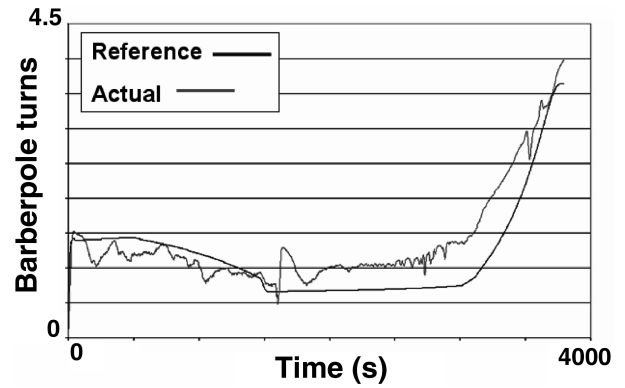


Fig. 26 Experimental results for the full functional tests.

between satellite and deployment rig), and included an advanced real-time space simulator that simulates a tether deployment in space, using orbital dynamics combined with the measured tension as actually established by the barberpole brake.

The satellite breadboard attempts to remain on track by measuring the deployed tether length and speed, comparing it with a reference table, and correcting the speed by changing the position of the barberpole tooth wheel (note there is no direct control of velocity, and the YES2 satellite has no tensiometer onboard so relies solely on its length sensors). Any dynamic system behavior or lack of control performance that would occur in space due to deviations in unwinding tension or the pole’s friction performance, bad control gains, or model errors, is thus realistically reproduced by the compact test rig.

The barberpole was able to successfully and accurately control the full 30 km deployment [18]. Figure 26 compares the model with the experimental result. The friction performance was adequately modeled and the number of turns of the pole generally deviates less than 0.5 turn from the nominal.

Conclusions

This paper presents the design of the YES2 barberpole brake, which is a simple, low-cost friction mechanism used to control deployment of a tether in space. It was found that the mechanism with a single gear and flexible coupling provides a good tradeoff for mechanical design complexity vs performance predictability and reliability. A large range of tensions can be achieved as it was demonstrated that an exponential relationship between input and output tension can be maintained. The mathematical model predicts that a nonstiff tether will remain in contact with the pole when deployed from a spool, independently of the speed, and the tether should follow a helical shape over the pole. The potential problem of overheating due to friction can be avoided by integrating the pole with a large exit side surface with good thermal contact. Experiments using a specially developed test rig on the ground, in vacuum and in zero *g* confirmed that these various conditions do not affect the performance significantly and ultimately showed the effectiveness of the brake at its task in controlling the first European tether deployment, YES2.

Appendix: Tether Tension Model

The tension of the tether around the barberpole was mathematically modeled considering different assumptions. In particular, the velocity of the tether around the pole *v*, the diameter of the tether *d*, the linear density of the tether ρ , the radius of the pole *r*, and the length of the pole *l* were considered constant. We also supposed that the tether had no bending stiffness and was always staying in contact with the pole during operations.

The forces acting on an infinitesimal tether length *ds* are the tension *T*, the normal force per unit length *N*, the friction force per unit length *fN*, and the inertial force of the tether (see Figs. A1 and A2).

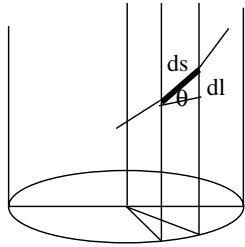


Fig. A1 Infinitesimal tether length ds on the pole.

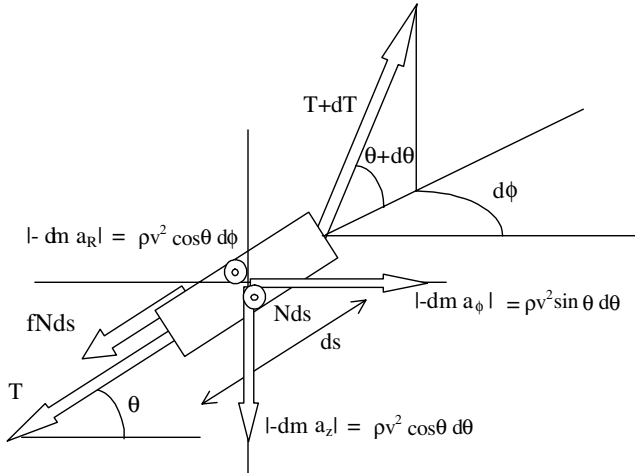


Fig. A2 Forces acting on an infinitesimal tether length.

For the sake of clarity, we also defined the variable R , and ϕ as

$$R = r + 0.5d \quad (\text{A1})$$

$$\phi = 2\pi n \quad (\text{A2})$$

where n is the number of pole turns.

Considering cylindrical coordinates, the radial force balance (see Fig. A2) is

$$N ds = (T + dT) \cos(\theta + d\theta) \sin d\phi \quad (\text{A3})$$

the tangential balance is

$$\begin{aligned} -\rho v^2 \sin \theta d\theta + (T + fN ds) \cos \theta \\ = (T + dT) \cos(\theta + d\theta) \cos d\phi \end{aligned} \quad (\text{A4})$$

and the balance in pole axis direction is

$$(T + fN ds) \sin \theta + \rho v^2 \cos \theta d\theta = (T + dT) \sin(\theta + d\theta) \quad (\text{A5})$$

Taking advantage of trigonometric identities, Eq. (A3) can be written as

$$N ds = (T - \rho v^2) \cos \theta d\phi \quad (\text{A6})$$

which, substituted into Eqs. (A5) and (A6), in a steady-state case ($\dot{v} = 0$), yields

$$d(T - \rho v^2)/(T - \rho v^2) = f \cos \theta d\phi + \tan \theta d\theta \quad (\text{A7})$$

$$d(T - \rho v^2)/(T - \rho v^2) = f \cos \theta d\phi - d\theta / \tan \theta \quad (\text{A8})$$

Equations (A7) and (A8) can be valid only if

$$d\theta \tan \theta = -d\theta / \tan \theta \quad (\text{A9})$$

that holds when $d\theta = 0$. Considering this result, the integration of Eq. (A9) yields

$$T = (T_0 - \rho v^2) e^{\cos \theta \int_{0,\phi}^f d\phi} + \rho v^2 \quad (\text{A10})$$

In the case of a constant friction coefficient f , Eq. (A10) can be simplified as

$$T = (T_0 - \rho v^2) e^{2\pi f n \cos \theta} + \rho v^2 \quad (\text{A11})$$

or alternatively as

$$T = (T_0 - \rho v^2) e^{2\pi f n \sqrt{(1/\{1+[1/2\pi n/(r+0.5d)]^2\})}} + \rho v^2 \quad (\text{A12})$$

which represent the tether tension model of the barberpole.

Acknowledgments

This work was possible due to the combined effort of a great many universities and students of the YES2 project. Thanks to Hans Rozemeijer [European Space Research and Technology Centre (ESTEC)] for his design suggestions; Ean Crellin at ESTEC for his mathematical support. Erik van der Heide (Delta-Utec), Angelos Miaris, and Dimitrios Lamprou (University of Patras) for their inputs; and to Ha-Min Chung (University of Remagen, Germany), Quentin Morel, Andrew Hyslop for excellent test work and support in development of the qualitative tether torque effect model; Massimo Busetto (Delta-Utec), Ferdi Hermanns and his students (Krefeld), for their contributions to the deployment testing work reported in this paper; Simone Lennert and Matthew Cartmell (Glasgow University) for their pioneering testing work; the YES2 zero g teams from FHS Remagen, Krefeld, Delta-Utec and Manitoba University (Canada); the 2nd Samara Space Summer School team at Samarskij Gosudarstvennyj Aerokosmiceskij Universitet (SSAU), Russia, for the vacuum chamber test; André Trévidic Nunes Tavares (ESTEC) for the pole roughness tests.

References

- [1] Ockels, W. J., van der Heide, E. J., and Kruijff, M., "Space Mail' and Tethers, Sample Return Capability for Space Station Alpha," IAF Paper 95-T.4.10, 1995.
- [2] Kruijff, M., and van der Heide, E. J., "YES2, the Second Young Engineers' Satellite A Tethered Inherently-Safe Re-Entry Capsule," IAC Paper 02-P.P.01., 2002.
- [3] Kruijff, M., "The Young Engineers' Satellite, Flight Results and Critical Analysis of a Super-Fast Hands-On Project," IAF Paper 99-P.1.04, 1999.
- [4] Kumar, K. D., "Review of Dynamics and Control of Non-electrodynamic Tethered Satellite Systems," *Journal of Spacecraft and Rockets*, Vol. 43, No. 4, 2006, pp. 705–720.
- [5] Bortolami, S. B., Lorenzini, E. C., Rupp, C. C., and Angrilli, F., "Control Law for the Deployment of SEDS II," *AAS/AIAA Astrodynamics Specialist Conference*, Vol. 85, Advances in the Astronautical Sciences, Astrodynamics, Univelt Inc. Publishers, AAS 93-706, 1993.
- [6] Glaese, J. R., "A Comparison of SEDS-2 Flight and Dynamics Simulation Results," *Proceedings of the Fourth International Conference on Tethers in Space*, Science and Technology Corp., Hampton, VA, April 1995.
- [7] van der Heide, E. J., Kruijff, M., Raitt, D., and Hermanns, F., "Space Spin-in from Textiles: Opportunities for Tethers and Innovative Technologies," IAC Paper 03-U.2.b.09, 2003.
- [8] Carroll, J., "SEDS Deployer Design and Flight Performance," AIAA 1993-4764, 1993.
- [9] Lorenzini, E. C., and Carroll, J., "In-Orbit Experimentation with the Small Expandable-Tether Deployment System," IAF Paper 90-048, 1990.
- [10] Carroll, J., and Oldson, J. C., "Tethers for Small Satellite Applications," *Proceedings of the 9th Annual AIAA/USU Conference on Small Satellites*, Logan, UT, 1995.
- [11] Kruijff, M., and van der Heide, E. J., "The YES Satellite: A Tethered Momentum Transfer in the GTO Orbit," *Proceedings of Tether Technology Interchange Meeting*, NASA CP-1998-206900, Jan. 1998.
- [12] Kruijff, M., and van der Heide, E. J., *Integrated Test Rig For Tether Hardware, Real-Time Simulator And Control Algorithms: Robust Momentum Transfer Validated*, STAIF, Albuquerque, NM, 2001.

- [13] Gavira, J., Rozemeijer, H., and Muencheberg, S., "The Tether System Experiment," ESA/ESTEC, ESA Bulletin 102, 2000.
- [14] van der Heide, E. J., and Kruijff, M., "StarTrack, A Swinging Tether Assisted Re-Entry for the International Space Station," ESTEC, ESA Working Paper 1883, March 1996.
- [15] Fortescue, P., Stark, J., and Swinerd, G., *Spacecraft Systems Engineering*, 3rd ed., Wiley, New York, 2005.
- [16] Kruijff, M., van der Heide, E. J., and Gil, S. C., "YES2 Inherently-Safe Tethered Re-Entry Mission and Contingencies," IAC Paper 03-IAA.6.2.02., 2003.
- [17] Gilmore, D. G., *Spacecraft Thermal Control Handbook*, 2nd ed., Vol. 1, AIAA, Reston, VA, 2002.
- [18] Hyslop, A., Kruijff, M., and Menon, C., "Simulating Space Tether Deployment on Earth for the YES2 Satellite," IAC Paper 05-A2.1.09., 2005.
- [19] Hyslop, A., Kruijff, M., van der Heide, E. J., Camps, C., and Timmermans, M., "Spool Winding and Deployment Testing for the YES2 Tethered Reentry Mission," *Proceedings of the 11th Australian International Aerospace Congress (AIAC-11)*, Melbourne, 2005.

G. Agnes
Associate Editor